ACS NANO

www.acsnano.org

ARTICLE

Single Mn Atom Doping in Chiral Sensitive Assembled Gold Clusters to Molecular Magnet

Deepak K. Swain, Gyanadeep Mallik, Pooja Srivastava, Anoop K. Kushwaha, Parasmani Rajput, Shambhu N. Jha, Seokmin Lim, Seungchul Kim, and Satchidananda Rath*

Cite This: *ACS Nano* 2021, 15, 6289–6295

Read Online

ACCESS | Metrics & More | Article Recommendations | Supporting Information

ABSTRACT: **Chiral stirred optical and magnetic properties, through the doping of assembled ultrasmall metal clusters (AMCs), are promising discernment to rivet the molecule-like quantum devices. Here, the single manganese (Mn) atom doping and assembly of the gold cluster (Au_8), leading to the chirality driven magnetism, has been achieved through a ligand-mediated growth. The X-ray absorption near edge structure and electron paramagnetic resonance studies corroborate the tetrahedral coordinated local structure of Mn dopant in the Au host. The optical and vibrational circular dichroic analysis affirms the modulation of chirality (negative to positive) in the presence of the Mn. A distinct ferromagnetic hysteresis loop at 300 K shows Mn ridden chiral sensitive ferromagnetism in contrary to the ligand influenced superparamagnetic undoped AMCs. The spin-polarized density functional theory level of calculations reveal the partial overlapping of spin-up and -down density of states in the doped AMCs, attributing to the ferromagnetic nature as like a molecular magnet suitable for the opto-spintronics application.**

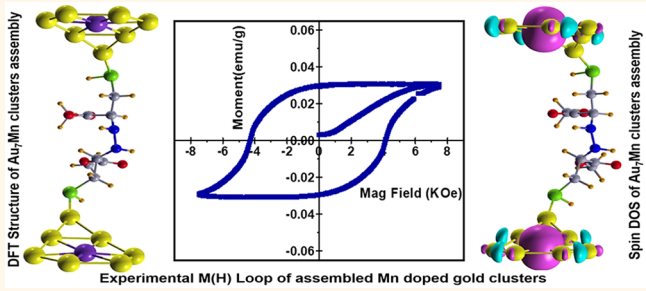

KEYWORDS: *gold cluster, molecular assembly, chiro-optical properties, magnetic properties, DFT calculation*

INTRODUCTION

The molecular origin of magnetism has triggered a surge of research interest, due to its phenomenal applications in high-density data storage,[1,2] quantum computing,[3] molecular spintronics,[4,5] and fast magnetic switches.[6,7] Ligand-coated metal oxide clusters,[8] multifunctional conducting molecules,[9] and organometallic compound[10] based single-molecule magnets (SMMs) showcase the quantum tunneling of magnetization, synergistic temperature dependent electrical and magnetic behavior, electrostatic interaction controlled magnetic anisotropy, *etc.*, while metal clusters (MCs) have been found to have excellent optical,[11] electrical,[12] and magnetic properties,[13] originating from the structural and orientational anisotropy of charge distributions of edge atoms to the vertex. Walt A. de. Heer *et al.*[14] observed multiferroic behavior in rhodium clusters despite the nonmagnetic nature of the bulk counterpart. Even so, the magnetism, emerging from the atomic-scale structured MCs, forms a stimulating subject of modern science and technology due to the adjustable properties emanating from the atomicity,[15] ligand-mediated interaction,[16] and tunable electronic structure.[17]

Recent studies illustrate the surface, interface, and structural ordering (chirality) driven spin−orbit coupled state of the carriers to the magnetic ground state,[18,19] due to the alteration of time-reversal symmetry. Concurrently, the chemical anisotropy, in terms of distance and composition, also manifests magnetic ordering. Further, the theoretical observations on the nonmagnetic atom doping in magnetic clusters[20] and magnetic atom doping in nonmagnetic clusters[21−23] (atomicity <12) show an enhanced magnetic moment due to the atom−cluster interaction mediated stability in the ground states and local electronic structures. At the same time, the triangular Fe- and Mn-germenides show topological chiral magnetism.[24] In spite of intriguing atom−cluster interaction mediated emerging properties, the preferential doping, leading to the change in chirality and magnetic exchange interaction, is rare in the literature. Meanwhile, the doping in ultrasmall MCs, where most of the atoms are believed to be surface atoms, is a challenging and subtle aspect, as the substitution of even a "single atom" could alter the geometry and hence the properties of the MCs. This study reports (i) the substitutional doping of a single manganese (Mn) atom in Au_8 clusters, (ii)

Received: December 8, 2020
Accepted: March 1, 2021
Published: March 5, 2021

https://dx.doi.org/10.1021/acsnano.0c10260
ACS Nano 2021, 15, 6289–6295

dopant-controlled chirality reconciled electronic and vibrational properties, and (iii) observation of room-temperature (300 K) ferromagnetic behavior, which are accomplished by the spin-polarized density functional theory (DFT) level of calculations.

RESULTS AND DISCUSSION

The atomicity, composition, and assembled structure of the gold cluster samples have been analyzed using matrix-assisted laser desorption time-of-flight (MALDI-TOF) mass spectrometry from a Bruker Reflex III Autoflex mass spectrometer attached with a nitrogen laser (337 nm). The data have been collected in positive linear mode from 3000 laser shots. Figure 1 shows the mass spectra of the MCs. Considering the mass of

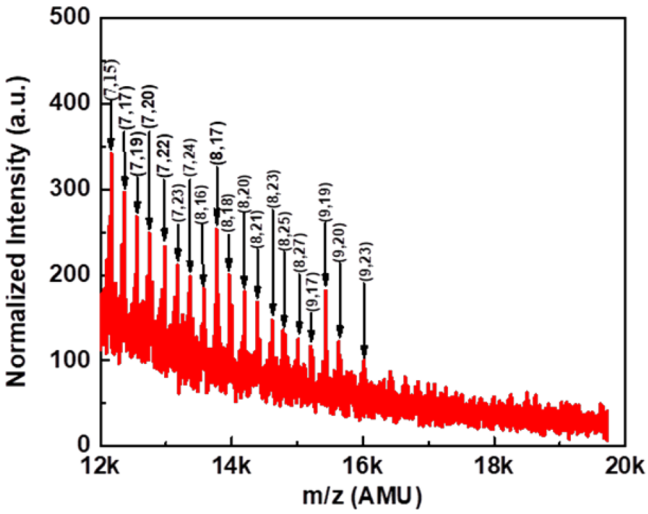

Figure 1. Matrix-assisted laser desorption time-of-flight mass spectrum of the Mn-doped gold clusters. The mass lines are leveled considering the units of the cluster (*m*) and ligand (*n*) as (*m*, *n*), respectively.

Mn, Au, and surfactant, the mass lines are leveled as (*m*, *n*), where "*m*" and "*n*" represent the number of units of Au_7Mn and L-cysteine methyl ester (LCME), respectively. The mass spectra, in the range of 12 to 20 K Da, contain a series of lines consisting of "*m*" from 7 to 9 and "*n*" from 15 to 23. Such a distribution may be due to the possible laser-induced fragmentation of the assembled clusters, which is a well-known phenomenon in mass spectrometry.[25,26] Comparing the intensity, the mass lines, referring to (7, 15), (8, 17), and (9, 19), are the most probable and stable clusters among various possibilities. Additionally, the mass line at (9, 23) pertained to the fairly unbroken structure of the pristine assembled metal clusters (AMCs), containing 9 units of Au_7Mn MCs, stabilized by 23 units of the LCME. However, considering the random nature of the laser-induced fragmentation, more high-resolution time-of-flight (TOF) is required to get further insight.

As the coordination of the dopant, in an ultrasmall cluster, plays a deciding role in electronic properties, hence, to identify the local structure of the dopant, X-ray absorption near-edge structure (XANES) measurements have been carried at the Mn K-edge, using the BL-9 beamline of the Indus-2 synchrotron center, RRCAT Indore, India. The Mn K-edge (6539 eV) excitation energy has been obtained from the synchrotron line, using a Rh/Pt-coated meridional cylindrical mirror for collimation and a Si(111) double-crystal monochromator. Figure 2a shows the XANES spectra of Au_7Mn, represented by the deep blue colored line. The black and red colored lines correspond to the MnO (Mn valence as 2^+) and Mn_2O_3 (Mn valence as 3^+) as a reference sample, respectively. In comparison with the reference data, the valence of the Mn dopant is affirmed to be Mn^{2+}. Further, the absence of a near-edge satellite-like pre-edge revealed the tetrahedral nature of the local structure of the dopant.[27] The local spin environment of the Mn dopant has also been analyzed using electron paramagnetic resonance (EPR) measurement at 300 K, and the corresponding spectrum is shown in Figure 2b. In spite of the low signal-to-noise ratio, a distinct spin splitting has been observed within a magnetic field range of 1500−6500 G. The effective Lande *g* factor (g_{eff}) of the sample is estimated to be 2.08. In general, the spin resonance line, with well-resolved five hyperfine structure (hfs), corresponding to g_{eff} = 2.0, is characteristics of the isolated Mn^{2+} ion. The wide and featureless spin states observed in our sample reveal the dipolar interaction mediated alteration of local structure around the Mn^{2+} site,[28] which is consistent with the XANES analysis.

Doping-regulated electronic properties of the AMCs have been studied using room-temperature (300 K) optical absorption and circular dichroic (absorption mode) measurements. Figure 3a shows the absorption spectrum of the Au_7Mn AMCs in a wavelength range of 200−1000 nm. A strong

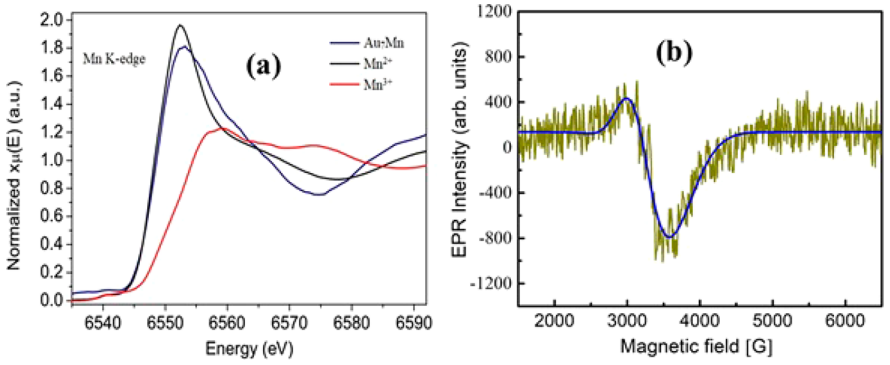

Figure 2. (a) Normalized X-ray absorption near-edge spectra (XANES) of the sample, Mn^{2+} reference, and Mn^{3+} reference, represented by blue, black, and red colored lines, respectively. (b) Electron paramagnetic resonance spectrum of the Au_7Mn AMCs. This measurement is carried out at a frequency of 9.44 GHz, and the effective Lande *g* factor is estimated to be 2.08. Blue line is the fitted curve.

https://dx.doi.org/10.1021/acsnano.0c10260
ACS Nano 2021, 15, 6289−6295

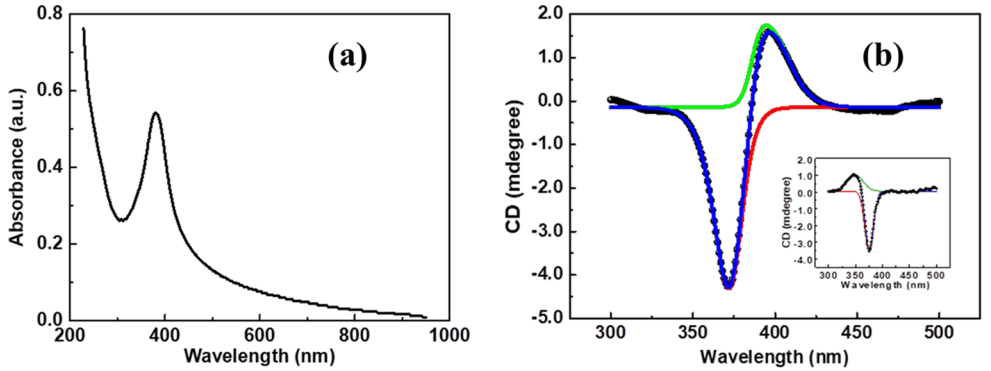

Figure 3. (a) Room-temperature optical absorption spectrum of the Au_7Mn AMCs. The sharp exciton peak appearing at 381 nm refers to the quantization of the sp band. (b) Circular dichroic (CD) spectra of the sample shown by a filled black circle. Red and green colored lines are the fitted curve of the doublet states. The blue curve is the resultant fitted line. Inset is the CD spectra of the Au_8 AMCs. The contrast in chirality is observed in the presence of the Mn dopant.

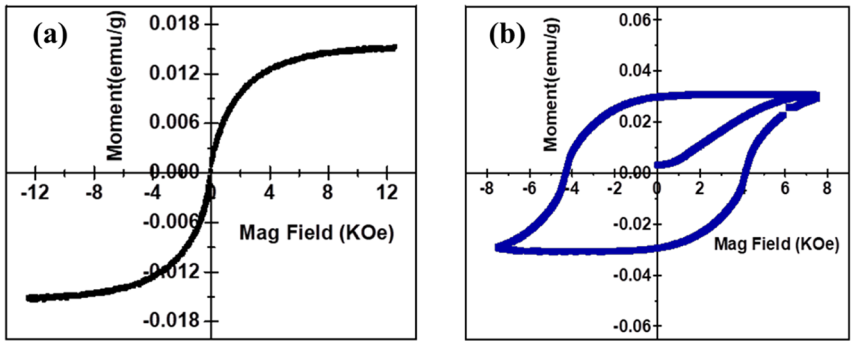

Figure 4. (a) *M versus H* plot of the Au_8 AMC sample at 300 K. The curve passing through the origin and attending saturation at a higher field reveals the superparamagnetic behavior with a saturation of magnetization, M_s, estimated as 0.015 emu/g. (b) Room-temperature *M versus H* plot of the Au_7Mn AMCs. A clear hysteresis loop with a coercive field of 4.23 kOe and remnant magnetization of 0.03 emu/g shows the ferromagnetic nature of the sample.

absorbance peak at 381 nm reveals a significant electronic transition referring to the distinct excitonic state emanating from the quantization of the sp conduction band and occupied d band of the gold.[29] The excitonic peak position is observed to be red-shifted in comparison to the Au_8, which may be due to the interaction of the Mn d-electrons with sp-electrons of gold, leading to a rearrangement of the electronic state in the presence of the Mn^{2+} state. Similarly, the shift in absorption band is common in the transition-metal-doped gold cluster.[30] The sharp absorption threshold confirms the uniformity in the size and composition of the MCs. Nevertheless, the absorption band has a spectral anisotropy toward the higher energy regime, which may be due to the superior electronic states. The electronic structure of the doped sample has further been analyzed using circular dichroic (CD) absorption measurements. Figure 3b shows the CD spectrum of the AMCs. It reveals the presence of a distinct doublet in the absorption band around the main absorption line. A weak and positive intensity line appeared at 395 nm, followed by a relatively stronger and negative intensity line observed at 372 nm. The doublet band, with contrasting CD indices, is apparent in the complex electric- and magnetic-dipole interactions in the AMCs.[31] As the system, responding to the circular polarized light in the higher wavelength zone, is regarded as the chirality,[31] the Au_7Mn AMCs exhibit positive chirality. Notably, the intensity of the negative CD index is more than the positive one, which may be due to the typical geometry-controlled dipole−dipole interaction.[31] The inset of Figure 3b shows the CD spectrum of Au_8 AMCs. In contrast to Au_7Mn AMCs, Au_8 exhibits negative chirality. This establishes that the Mn dopant did modify the chirality of the gold clusters.

According to Rikken *et al.*,[32] the subtle chiral electronic structure favors magnetic ordering. The impact of the handedness on the magnetic properties of the gold AMCs has been studied, using the Quantum Design Dynacool vibrating sample magnetometer setup. Figure 4b shows the magnetization (M) *versus* applied magnetic field (H) plot of the doped AMCs at 300 K. A clear hysteresis loop with remanence magnetization (M_r) of 0.03 emu/g and a coercivity field (H_c) of 4.23 kOe reveal the ferromagnetic behavior of the sample. On the contrary, Figure 4a exhibits a reversible S-shaped incremental change in the $M-H$ curve that is passing through the origin with the field, followed by saturation of magnetization (M_s), 0.015 emu/g. It reveals the superparamagnetic (SPM) nature of the undoped sample. A similar M_s is commonly observed in gold nanoparticles.[33] In order to understand the origin of magnetism, there are contemporary theories, *viz.*, (i) the thiol-containing ligand protected gold cluster exhibits ferromagnetism due to the 5d-localized holes arising from Au−S bonding,[34] whereas (ii) Hori *et al.*[35] describes ferromagnetic properties of weakly protected gold nanoparticles, due to the size-dominated Fermi-hole effect, and (iii) both the size confinement effect and dilute assembly often yield SPM properties.[36,37] Thus, the SPM characteristics observed in the Au_8 AMCs is purely due to the structural origin. Similarly, the ferromagnetic nature of Mn-doped AMCs

https://dx.doi.org/10.1021/acsnano.0c10260
ACS Nano 2021, 15, 6289−6295

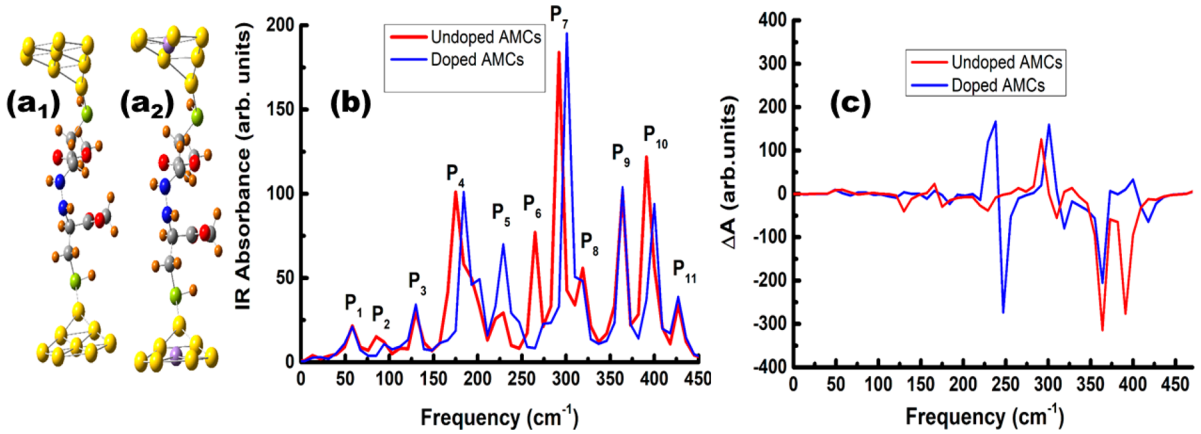

Figure 5. Optimized structure of (a_1) AMCs and (a_2) Mn-doped AMCs. The red, orange, yellow, green, blue, violet, and gray spheres represent oxygen, hydrogen, gold, sulfur, nitrogen, manganese, and carbon atoms, respectively. Infrared absorption (b) and vibrational circular dichroic (c) spectra of the doped AMCs and undoped AMCs represented by blue and red colored lines, respectively.

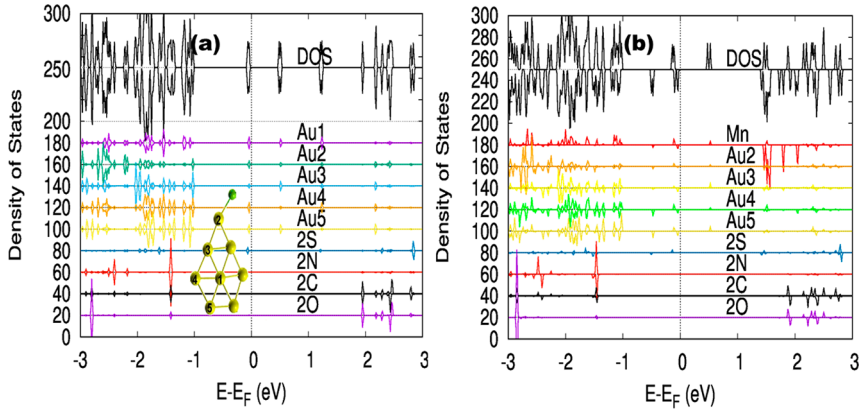

Figure 6. (a) Calculated density of state (DOS) and partial density of state (PDOS) spectra of Au_8 AMCs. Inset of (a) shows the positions of Au for which the partial density of state (PDOS) is calculated. The overlapping of the upper and lower DOS near the Fermi level is attributed to the paramagnetic properties. (b) DOS and PDOS of Mn-doped AMCs. Here, the PDOS is estimated by substituting the Au1 position by Mn. The partial overlapping of the upper and lower DOS near the Fermi level indicates the ferromagnetic nature. As spins in O, N, and S are also polarized, the tails of the spin magnetic moments from two metal clusters are connected, indicating ferromagnetic coupling between two metal clusters.

is due to the Mn-mediated sp−d interaction and fixed chiral electronic structure.

To infer the origin of the structural and electronic chirality driven magnetic properties, we have performed vibrational circular dichroic (VCD) and spin-polarized electronic density of states (DOS) calculation, using DFT, as implemented in the Gaussian package and Vienna ab Initio Simulation Package (VASP),[38] respectively, for the optimized structure. The geometry optimization protocol proceeds in three steps, *viz.*, optimization of (1) Au_8 structure, (2) two ligand-protected Au_8, and (3) substitutional Mn doping in ligand-protected Au_8. To test the accuracy of chosen GGA (PAW−PBE) functional, we have verified the ground-state geometry for a capped hexagonal structure of Au_8 and Au_7Mn AMCs, which are in excellent agreement with the results obtained by H. Baek *et al.*[39] Considering the experimental results and limitation of the computational calculation timing, the "two clusters separated by two LCME ligand molecules" (*e.g.*, 2-(LCME-Au_8) and 2-(LCME-Au_7Mn)) are taken as the unit cell within a periodic boundary condition for DFT level calculation. Figure 5a_1 and a_2 are the optimized structures of the undoped and Mn-doped AMCs, respectively. The geometry optimization details are available in the Supporting Information (Figures S1−S3).

The VCD analysis is a sensitive approach to understand the structural chirality through absorption of circularly polarized light in the infrared (IR) regime. Figure 5b and c show the calculated IR and VCD spectra of doped and undoped AMCs, indicated by blue and red colored lines, respectively. As shown in Figure 5b, the calculated IR absorption spectra contain promising Au−Au, Au−S (sulfur), and ligand−ligand absorption bands, in the frequency range 0−450 cm^{-1}. The IR vibration spectra yield a series of peaks at P_1 (60 cm^{-1}), P_2 (85 cm^{-1}), P_3 (130 cm^{-1}), P_4 (174 cm^{-1}), P_5 (230 cm^{-1}), P_6 (265 cm^{-1}), P_7 (293 cm^{-1}), P_8 (319 cm^{-1}), P_9 (363 cm^{-1}), P_{10} (391 cm^{-1}), and P_{11} (428 cm^{-1}). The origin of the IR peak has been analyzed and assigned from the real-time vibration of optimized structure. Here, P_1 and P_2 refer to the bending mode of the Au (core)−S (staple) bond and the Au−Au stretching mode, respectively. Again, the peak P_4 is assigned to the collective mode of vibration of the Au (core)−ligand bonds. The peak P_5 is assigned to the rocking mode of vibration of the carbon−hydrogen bond present in the ligand. Interestingly, the intensity of the same mode increased significantly in the presence of Mn dopant, due to the additional contribution of a Au−Mn−Au asymmetric stretching vibration in the same band. The P_6 band may be due to the C−C bending mode of

https://dx.doi.org/10.1021/acsnano.0c10260
ACS Nano 2021, 15, 6289−6295

the vibration. The intense IR peaks P_7 and P_8 can be assigned to the radial and tangential modes of the vibration of the Au−S bond, respectively. Similar vibrations have been observed by T. Burgi *et al.*,[40] from the thiolated ligand protected Au_{25} clusters. At the same time, the peaks P_3, P_9, and P_{11}, having nearly the same intensity, originate from the collective vibration of ligand−ligand bonds. The P_{10} band refers to the in-plane vibration of the Au−S−C bond. Notably, in comparison to the undoped sample, the IR bands P_2, P_4, P_7, and P_{10} of the doped AMCs are shifted to higher frequency by 10 cm^{-1}, which may be due to the presence of the Mn-modified Au−S bond length or the effect of the lighter mass of Mn than Au. Figure 5c shows the VCD spectra of AMCs and doped AMCs, represented by red and blue colored lines, respectively. A flip-over chirality has been observed around the IR bands P_5 and P_{10} in the case of doped AMCs, in contrast to the AMCs. According to Rosenfeld's formula, the VCD absorption,[41] R_{ab}, is related to the vibration mode corresponding to the transition from state "a" to "b" by $R_{ab} = \mathbb{I}m\{\langle a|\mu_e|b\rangle\langle b|\mu_m|a\rangle\}$, where the electric dipole operator of the molecule-like system is $\mu_e = \sum_k q_k r_k \mu_k$, and q_k, r_k, and μ_k are the charge, position operator, and magnetic dipole operator of the kth particle of the molecule-like system. The electric and magnetic dipole are related through the Born−Oppenheimer (BO) approximation, which states that the total wave function is the product of the nuclear and electron wave function, through a perturbational approach (*e.g.*, magnetic field perturbational approach).[42] Therefore, the promising flip-over chirality (negative to positive) dominated IR band (peak P_5) indicates a Au−Mn−Au vibration, which induces strong overlapping of the Mn state function with Au to a finite magnetic dipole moment. Figure 6a and b show the calculated spin-polarized DOS and partial density of states (PDOS) spectra of the AMCs and doped AMCs, respectively. In the case of Mn-doped AMCs, the DOS and PDOS affirm the partial overlapping of the upper and lower DOS near the Fermi level, with the up- and down-spin states present at different energies (spin gap ∼0.44 eV). Considering the same (FM ordering) and opposite (AFM ordering) spin configuration, the calculated spin energy of the Mn atom is found to be ∼0.74 eV/fu (fu = formula unit), which is lower than the AFM ordering of the same. This strongly reveals the presence of ferromagnetic ordering due to atom−cluster interactions. In our study, the major contribution to the magnetic moment is arising from the Mn states, and a minor contribution to the same is coming from the Au states. However, the Mn and Au states are antiferromagnetically coupled. This suggests the C/O/S/N atoms (ligands), which are in the middle of two MCs, also acquire a tiny magnetic moment (Supporting Information, Figure S4), indicating the ferromagnetic coupling between two MCs, through the spatially connected tails of magnetic states. At the same time, the full overlapping of the upper and lower DOS near the Fermi level of undoped AMCs can be attributed to the nonmagnetic properties. Figure 7 shows the contour plot of the spin-density of the Mn-doped AMCs, referring to the spin-up and spin-down states, marked by cyan and violet colors, respectively. The spin-density isosurface is plotted at an isovalue of 2×10^{-2} e per $Å^3$. The spin-down states, appearing almost at the Fermi level, are mainly contributed by the d-orbitals of Mn atom.

On the other hand, for the undoped samples, there is a discrepancy between theoretical and experimental results. At the same time, there are several experimental evidences[33−36]

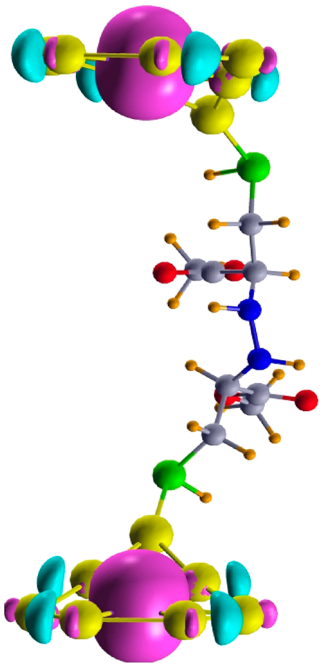

Figure 7. Spin-density of state referring to the spin-up and spin-down states of the optimized structure of doped Au AMCs, shown by cyan and violet colored contour plots, respectively. Spin-density isosurface for undoped and doped clusters plotted at an isovalue of 2×10^{-2} e per $Å^3$. The spin-density of states on the ligand is not visible due to the very low order ($\sim 10^{-5}$) of the isovalue.

confirming the thiolated ligand surface-passivated gold nanoclusters retain magnetic properties due to the charge sharing by the Au−S interaction. From the spin-DOS contour plot (Supporting Information, Figure S4), we have also observed a very weak spin-density distribution around the S-site. Hence, the deviation of our calculated results of undoped AMCs from the experiment may be due to the absence of a sufficient number of Au−S interaction terms, where a small part of the experimentally observed structure is considered for calculation to gain qualitative information.

CONCLUSIONS

In summary, the single Mn atom doping in ligand-protected and assembled Au_8 clusters, carrying chiral dominated properties, has been achieved through a wet chemical route. The time-of-flight mass spectrometry confirms the self-assembly of the ligand-protected metal clusters. As observed from the XANES and EPR, the Mn dopant occupied the tetrahedral position in the Au host. The CD and VCD analyses revealed the dopant-mediated alteration of the electronic and structural chirality of the samples. The magnetic measurements of positive chiral Mn-doped gold clusters accomplished the room temperature ferromagnetic hysteresis loop ($M_r \approx 0.03$ emu/g, $H_c \approx 4.23$ kOe), in contrast to negative chiral gold clusters with superparamagnetic properties (M_s is estimated to be 0.015 emu/g). The spin-polarized density functional theory level of calculation complements the Mn-dominated ferromagnetic property of the assembled gold clusters as a molecular magnet. This work enables realizing the atom−cluster interaction phenomena in the ligand−metal cluster assembly to a chiral magnetic material for opto-spintronics applications.

https://dx.doi.org/10.1021/acsnano.0c10260
ACS Nano 2021, 15, 6289−6295

EXPERIMENTAL SECTION

The Mn-doped gold nanoclusters (Au_7Mn) have been prepared through a modified ligand-mediated chemical reduction of Au ions in an aqueous medium.[43] The precursors used are gold chloride tetrahydrate ($HAuCl_4{\cdot}4H_2O$) as the metal source, manganese chloride as a source of Mn dopant, LCME as the surfactant, and sodium borohydride ($NaBH_4$) as the reducing agent, respectively. For a typical synthesis, 100 μL of a 0.06 M aqueous gold solution was added dropwise (20 μL/20 min) to a 0.02 M LCME solution under vigorous stirring, followed by dropwise addition of 100 μL of the 0.008 M manganese chloride solution, as an optimized salt concentration. To achieve a complete reduction of the metal ions, 140 μL of 0.04 M $NaBH_4$ was added dropwise (20 μL/5 min) to the resultant solution. After 30 min of the reduction reaction, the solution was maintained at a temperature of 330 K for 40 min, under vigorous stirring conditions ensued by overnight stirring at 300 K, to facilitate nucleation, growth, and self-assembly. The Mn-doped and assembled Au cluster (Au_7Mn), in powder form, was collected by selective precipitation and centrifuging from the final solution. The sample was washed repeatedly with deionized water and absolute ethanol to get rid of unreacted ions/ligands (if any) followed by vacuum drying in a desiccator. The powder samples were characterized using matrix-assisted laser desorption time-of-flight (MALDI-TOF) mass spectrometry, XANES, EPR, CD absorption, and magnetic measurements using a physical properties measurement system, containing a superconducting magnet.

ASSOCIATED CONTENT

Supporting Information

The Supporting Information is available free of charge at https://pubs.acs.org/doi/10.1021/acsnano.0c10260.

DFT-based geometry optimization of six ligand-Au_7Mn cluster (Figure S1), 2 ligand-2 Au_8 (Figure S2), and 2 ligand-2 Au_7Mn (Figure S3), tabulated data showing the optimization of energy and magnetic moment (Table S1), and contour plot of spin density of states of the 2 ligand-2 Au_8 cluster assembly (Figure S4) (PDF)

AUTHOR INFORMATION

Corresponding Author

Satchidananda Rath − *School of Basic Sciences, Indian Institute of Technology Bhubaneswar, Argul Jatni 752050, India;* orcid.org/0000-0002-9017-1799; Email: srath@iitbbs.ac.in

Authors

Deepak K. Swain − *School of Basic Sciences, Indian Institute of Technology Bhubaneswar, Argul Jatni 752050, India;* orcid.org/0000-0003-0776-2553

Gyanadeep Mallik − *School of Basic Sciences, Indian Institute of Technology Bhubaneswar, Argul Jatni 752050, India*

Pooja Srivastava − *Department of Physics, Amity University, Lucknow 226010, India*

Anoop K. Kushwaha − *School of Basic Sciences, Indian Institute of Technology Bhubaneswar, Argul Jatni 752050, India*

Parasmani Rajput − *Beamline Development and Application Section, Bhabha Atomic Research Centre, Mumbai 400085, India*

Shambhu N. Jha − *Beamline Development and Application Section, Bhabha Atomic Research Centre, Mumbai 400085, India*

Seokmin Lim − *Korea Institute of Science and Technology, Seoul 02792, Republic of Korea; Division of Nano and Information Technology, University of Science and Technology, Daejeon 34113, Republic of Korea*

Seungchul Kim − *Korea Institute of Science and Technology, Seoul 02792, Republic of Korea*

Complete contact information is available at: https://pubs.acs.org/10.1021/acsnano.0c10260

Author Contributions

S.R., D.K.S., and G.M designed the project and work plan, carried out the experiment for sample preparation, chiral optical studies, MALDI studies, and EPR studies, plotted the figures, analyzed the results and wrote the manuscript. P.S. and S.K. helped with DFT calculations and analysis. P.R. and S.N.J. helped with XANES measurements and analysis, and A.K.K helped with VCD calculations. The input of all the authors is included in the manuscript.

Notes

The authors declare no competing financial interest.

ACKNOWLEDGMENTS

S.R. acknowledges the financial support received from the Nanomission, DST India, under the scheme SR/NM/NS-68/2016 (G). S.R. thanks Dr. N. Mohapatra for extending the support for magnetic measurements. P.S. and S.K. thank the amber cluster facility of Korean Institute of Science and Technology. S.K. also thanks the support provided by the KIST Institutional project (grant no. 2E30460), and P.S. acknowledges the support provided by SERB grant TAR/2018/000834.

REFERENCES

(1) Natterer, F. D.; Yang, K.; Paul, W.; Willke, P.; Choi, T.; Greber, T.; Heinrich, A. J.; Lutz, C. P. Reading and Writing Single-Atom Magnets. *Nature* **2017**, *543* (7644), 226−228.

(2) Affronte, M. Molecular Nanomagnets for Information Technologies. *J. Mater. Chem.* **2009**, *19* (12), 1731−1737.

(3) Leuenberger, M. N.; Loss, D. Quantum Computing in Molecular Magnets. *Nature* **2001**, *410* (6830), 789−793.

(4) Donati, F.; Rusponi, S.; Stepanow, S.; Wäckerlin, C.; Singha, A.; Persichetti, L.; Baltic, R.; Diller, K.; Patthey, F.; Fernandes, E.; Dreiser, J.; Šljivančanin; Kummer, K.; Nistor, C.; Gambardella, P.; Brune, H. Magnetic Remanence in Single Atoms. *Science (Washington, DC, U. S.)* **2016**, *352* (6283), 318−321.

(5) Bogani, L.; Wernsdorfer, W. Molecular Spintronics Using Single-Molecule Magnets. In *Nanoscience and Technology: A Collection of Reviews from Nature Journals*; World Scientific Publishing Co.: UK, 2009; pp 194−204.

(6) Misiorny, M.; Barnaś, J. Magnetic Switching of a Single Molecular Magnet Due to Spin-Polarized Current. *Phys. Rev. B: Condens. Matter Mater. Phys.* **2007**, *75* (13), 134425.

(7) Johansson, J. O.; Kim, J. W.; Allwright, E.; Rogers, D. M.; Robertson, N.; Bigot, J. Y. Directly Probing Spin Dynamics in a Molecular Magnet with Femtosecond Time-Resolution. *Chem. Sci.* **2016**, *7* (12), 7061−7067.

(8) Soler, M.; Wernsdorfer, W.; Folting, K.; Pink, M.; Christou, G. Single-Molecule Magnets: A Large Mn_{30} Molecular Nanomagnet Exhibiting Quantum Tunneling of Magnetization. *J. Am. Chem. Soc.* **2004**, *126* (7), 2156−2165.

(9) Cosquer, G.; Shen, Y.; Almeida, M.; Yamashita, M. Conducting Single-Molecule Magnet Materials. *Dalt. Trans.* **2018**, *47* (23), 7616−7627.

(10) Baldoví, J. J.; Clemente-Juan, J. M.; Coronado, E.; Gaita-Ariño, A. Molecular Anisotropy Analysis of Single-Ion Magnets Using an Effective Electrostatic Model. *Inorg. Chem.* **2014**, *53* (20), 11323−11327.

(11) Rath, S.; Halder, O.; Pradhani, A.; Satpati, B.; Maity, A.; Chini, T. K.; Gogurla, N.; Ray, S. K. White-Light Emission by Phonon Assisted Coherent Mixing of Excitons in Au_8-CdS Hybrid Nanorods. *Nanotechnology* **2016**, *27* (49), 495706.
(12) Wang, J.; Wang, G.; Zhao, J. Density-Functional Study of Au_n (n = 2−20) Clusters: Lowest-Energy Structures and Electronic Properties. *Phys. Rev. B - Condens. Matter Mater. Phys.* **2002**, *66* (3), 1−6.
(13) Ojeda-López, M. A. Noncollinear Magnetic Order in Antiferromagnetic and Weak-Ferromagnetic Transition-Metal Clusters. *Solid State Commun.* **2000**, *114* (6), 301−304.
(14) Ma, L.; Moro, R.; Bowlan, J.; De Heer, W. A. Multiferroic Rhodium Clusters. *Phys. Rev. Lett.* **2014**, *113* (15), 157203.
(15) Magyar, R. J.; Mujica, V.; Marquez, M.; Gonzalez, C. Density-Functional Study of Magnetism in Bare Au Nanoclusters: Evidence of Permanent Size-Dependent Spin Polarization without Geometry Relaxation. *Phys. Rev. B: Condens. Matter Mater. Phys.* **2007**, *75* (14), 144421.
(16) Yamamoto, Y.; Miura, T.; Suzuki, M.; Kawamura, N.; Miyagawa, H.; Nakamura, T.; Kobayashi, K.; Teranishi, T.; Hori, H. Direct Observation of Ferromagnetic Spin Polarization in Gold Nanoparticles. *Phys. Rev. Lett.* **2004**, *93* (11), 116801.
(17) Ayuela, A.; Crespo, P.; García, M. A.; Hernando, A.; Echenique, P. M. Sp Magnetism in Clusters of Gold Thiolates. *New J. Phys.* **2012**, *14* (1), 013064.
(18) Martin, I.; Batista, C. D. Itinerant Electron-Driven Chiral Magnetic Ordering and Spontaneous Quantum Hall Effect in Triangular Lattice Models. *Phys. Rev. Lett.* **2008**, *101* (15), 156402.
(19) Streubel, R.; Lambert, C. H.; Kent, N.; Ercius, P.; N'Diaye, A. T.; Ophus, C.; Salahuddin, S.; Fischer, P. Experimental Evidence of Chiral Ferrimagnetism in Amorphous GdCo Films. *Adv. Mater.* **2018**, *30* (27), 1800199.
(20) Kabir, M.; Kanhere, D. G.; Mookerjee, A. Emergence of Noncollinear Magnetic Ordering in Small Magnetic Clusters Mn_n and As@Mn_n. *Phys. Rev. B: Condens. Matter Mater. Phys.* **2007**, *75* (21), 214433.
(21) Ehlert, C.; Hamilton, I. P. Iron Doped Gold Cluster Nanomagnets: *ab Initio* Determination of Barriers for Demagnetization. *Nanoscale Adv.* **2019**, *1* (4), 1553−1559.
(22) Zhang, M.; He, L. M.; Zhao, L. X.; Feng, X. J.; Luo, Y. H. Tuning Magnetic Moments by 3D Transition-Metal-Doped Au_6 Clusters. *J. Phys. Chem. C* **2009**, *113* (16), 6491−6496.
(23) Du, Q.; Wu, X.; Wang, P.; Wu, D.; Sai, L.; King, R. B.; Park, S. J.; Zhao, J. Structure Evolution of Transition Metal-Doped Gold Clusters M@Au_{12} (M = 3D-5D): Across the Periodic Table. *J. Phys. Chem. C* **2020**, *124* (13), 7449−7457.
(24) Grytsiuk, S.; Hanke, J. P.; Hoffmann, M.; Bouaziz, J.; Gomonay, O.; Bihlmayer, G.; Lounis, S.; Mokrousov, Y.; Blügel, S. Topological−Chiral Magnetic Interactions Driven by Emergent Orbital Magnetism. *Nat. Commun.* **2020**, *11* (1), 511.
(25) Dass, A.; Stevenson, A.; Dubay, G. R.; Tracy, J. B.; Murray, R. W. Nanoparticle MALDI-TOF Mass Spectrometry without Fragmentation: $Au_{25}(SCH_2CH_2Ph)_{18}$ and Mixed Monolayer $Au_{25}(SCH_2CH_2Ph)_{18-X}(L)_X$. *J. Am. Chem. Soc.* **2008**, *130* (18), 5940−5946.
(26) Tsunoyama, H.; Tsukuda, T. Magic Numbers of Gold Clusters Stabilized by PVP. *J. Am. Chem. Soc.* **2009**, *131* (51), 18216−18217.
(27) Goncharuk, N. A.; Kucera, J.; Smrcka, L. Pre-Edge XANES Structure of Mn in (Ga,Mn)As from First Principles. *Chem. Met. Alloy* **2009**, *2* (1/2), 34−38.
(28) Halder, O.; Satpati, B.; Rajput, P.; Mohapatra, N.; Jha, S. N.; Suffczyński, J.; Pacuski, W.; Rath, S. Light Emitting Spin Active Electronic States in Ultra-Thin Mn Doped CdSe Layered Nanosheets. *Sci. Rep.* **2019**, *9* (1), 1804.
(29) Liu, L.; Zheng, H. Z.; Zhang, Z. J.; Huang, Y. M.; Chen, S. M.; Hu, Y. F. Photoluminescence from Water-Soluble BSA-Protected Gold Nanoparticles. *Spectrochim. Acta, Part A* **2008**, *69* (3), 701−705.
(30) Negishi, Y.; Munakata, K.; Ohgake, W.; Nobusada, K. Effect of Copper Doping on Electronic Structure, Geometric Structure, and Stability of Thiolate-Protected Au_{25} Nanoclusters. *J. Phys. Chem. Lett.* **2012**, *3* (16), 2209−2214.
(31) Berova, N.; Di Bari, L.; Pescitelli, G. Application of Electronic Circular Dichroism in Configurational and Conformational Analysis of Organic Compounds. *Chem. Soc. Rev.* **2007**, *36* (6), 914−931.
(32) Rikken, G. L. J. A.; Raupach, E. Enantioselective Magnetochiral Photochemistry. *Nature* **2000**, *405* (6789), 932−935.
(33) Nealon, G. L.; Donnio, B.; Greget, R.; Kappler, J.-P.; Terazzi, E.; Gallani, J.-L. Magnetism in Gold Nanoparticles. *Nanoscale* **2012**, *4* (17), 5244.
(34) Negishi, Y.; Tsunoyama, H.; Suzuki, M.; Kawamura, N.; Matsushita, M. M.; Maruyama, K.; Sugawara, T.; Yokoyama, T.; Tsukuda, T. X-Ray Magnetic Circular Dichroism of Size-Selected, Thiolated Gold Clusters. *J. Am. Chem. Soc.* **2006**, *128* (37), 12034−12035.
(35) Hori, H.; Yamamoto, Y.; Iwamoto, T.; Miura, T.; Teranishi, T.; Miyake, M. Diameter Dependence of Ferromagnetic Spin Moment in Au Nanocrystals. *Phys. Rev. B: Condens. Matter Mater. Phys.* **2004**, *69* (17), 174411.
(36) Chen, D. X.; Sanchez, A.; Taboada, E.; Roig, A.; Sun, N.; Gu, H. C. Size Determination of Superparamagnetic Nanoparticles from Magnetization Curve. *J. Appl. Phys.* **2009**, *105* (8), 083924.
(37) Kwon, K. C.; Jo, E.; Kwon, Y. W.; Lee, B.; Ryu, J. H.; Lee, E. J.; Kim, K.; Lee, J. Superparamagnetic Gold Nanoparticles Synthesized on Protein Particle Scaffolds for Cancer Theragnosis. *Adv. Mater.* **2017**, *29* (38), 1701146.
(38) Kresse, G.; Furthmüller, J. Efficiency of *ab Initio* Total Energy Calculations for Metals and Semiconductors Using a Plane-Wave Basis Set. *Comput. Mater. Sci.* **1996**, *6* (1), 15−50.
(39) Baek, H.; Moon, J.; Kim, J. Benchmark Study of Density Functional Theory for Neutral Gold Clusters, Au_n (n = 2−8). *J. Phys. Chem. A* **2017**, *121* (12), 2410−2419.
(40) Dolamic, I.; Varnholt, B.; Bürgi, T. Far-Infrared Spectra of Well-Defined Thiolate-Protected Gold Clusters. *Phys. Chem. Chem. Phys.* **2013**, *15* (45), 19561−19565.
(41) Magyarfalvi, G.; Tarczay, G.; Vass, E. Vibrational Circular Dichroism. *Wiley Interdiscip. Rev. Comput. Mol. Sci.* **2011**, *1* (3), 403−425.
(42) Stephens, P. J. Theory of Vibrational Circular Dichroism. *J. Phys. Chem.* **1985**, *89* (5), 748−752.
(43) Rath, S.; Nozaki, S.; Palagin, D.; Matulis, V.; Ivashkevich, O.; Maki, S. Aqueous-Based Synthesis of Atomic Gold Clusters: Geometry and Optical Properties. *Appl. Phys. Lett.* **2010**, *97* (5), 053103.

https://dx.doi.org/10.1021/acsnano.0c10260
ACS Nano 2021, 15, 6289−6295